Communication 1

CHAIRE DE CONSTRUCTIONS HYDRAULIQUES

Département de Génie Civil

Ecole Polytechnique Fédérale de Lausanne

DISCHARGE MEASUREMENT STRUCTURES

W. H. Hager

Titulaire de la Chaire :

Prof. R. Sinniger

LAUSANNE 1986

Preface

Discharge measurement is as old as hydraulics; indeed, the first hydraulicians have been attracted by the question of how much water is running in a conduit or in a channel. Today, the quantity of flow is determined with a large number of different devices, each having its particular advantage.

The purpose of the present investigation is to review the most important discharge measurement structures used in current engineering applications. Computational details and descriptions of experimental facilities are thereby largely ignored in order to stress on the principles of discharge measurements and provide insight in the governing equations, by which the discharge can be determined. This review may serve as a guide to hydraulicians, since the fundamental theory of critical flow is developped in detail as well as to the practitioneer, to whom the procedure of evaluating discharge is explained by diagrams and illustrated by typical examples.

This study has been supported by Prof. R. Sinniger, Chair of Hydraulic Constructions, EPFL. The author would like to acknowledge the review of the manuscript by PD Dr. K. Hutter, VAW, ETH-Zürich. Finally, thanks to Mrs. M.-L. Tanner for typing the manuscript.

Willi H. Hager

Lausanne, 1986

Abstract

The discharge characteristics of the important discharge measurement structures in civil engineering applications are presented. Using the theory of the critical flow conditions, the governing relations for the upstream flow depth-discharge relations are derived for weir and flume type devices. These computations are based on the hydrostatic pressure and uniform velocity distribution concept; for flows in which the streamline curvature becomes significant, a more general, quasi two-dimensional approach is presented. The results are applied to discharge measurement structures of which the geometry is slightly and moderately varied. For rapidly varied channel geometry, such as for thin plate weirs, a semi-empirical approach is chosen. All results are represented graphically and typical examples illustrate the computational procedure to evaluate the discharge characteristics of thestructures discussed.

Résumé

Les caractéristiques du débit sont présentées pour les structures de jaugeage dans le domaine du génie civil. Les relations entre la hauteur d'eau à l'amont de la structure et le débit pour les déversoirs et les canaux type Venturi sont déterminées en tenant compte de la condition d'écoulement critique. Ces calculs se basent sur les hypothèses de répartition hydrostatique des pressions et uniforme des vitesses; pour les écoulements dont la courbure des lignes de courants est importante, une approche quasi bidimensionnelle est choisie. Les résultats qui en découlent s'appliquent à des structures où le changement longitudinal de la géométrie est faible ou modéré. Pour des structures à changement rapide de la géométrie, comme par exemple les déversoirs à mince crête, une approche semi-empirique est préférée. Tous les résultats sont représentés prêts à l'application; la marche à suivre du calcul pour les structures de jaugeage discutées est illustrée par des exemples types.

Zusammenfassung

Die Durchfluss-Charakteristika der wichtigsten Abflussmessanlagen des Ingenieurwesens werden vorgestellt. Aufgrund der kritischen Abflusstheorie sind die grundlegenden Beziehungen zwischen Oberwassertiefe und Durchfluss für Wehre und Venturikanäle abgeleitet. Diese Berechnungen basieren auf der Annahme hydrostatischer Druck- und uniformer Geschwindigkeits-Verteilungen; Abflüsse, bei denen der Einfluss der Stromlinienkrümmung entscheidend ist, werden unter Zuhilfenahme eines quasi-zweidimensionalen Verfahrens vorgestellt. Die sich ergebenden Resultate lassen sich auf Durchfluss-Messanlagen anwenden, deren Kanalgeometrie schwachen und mittleren Längsänderungen unterliegt. Für abrupt ändernde Kanalgeometrie, beispielsweise dünnwandige Messwehren, wird eine halbempirische Berechnungsmethode verfolgt. Alle Resultate sind anwendungsbezogen dargestellt; typische Beispiele zeigen den Berechnungsweg zur Ermittlung der Durchfluss-Eigenschaft der diskutierten Bauwerke auf.

Contents

1. INTRODUCTION

Flow of water is closely related to energy production, drinking water consumption and water flow in sewers, among others. Evidently it is not only important to know that water is available but also how much water is flowing. Therefore, discharge measurement is as old as the first channels designed in antiquity. Some well-known devices are the so-called "water clocks", or discharge measurement orifices. For larger quantities, these must be replaced by more appropriate devices; some of the most important will be discussed herein.

Discharge may be measured by a large variety of methods, owing to the precision desired and the installations available. High precision for low and moderate discharge provide so-called Thomson triangular thin plate weirs, while the dilution method is recommended rather for small streams with low requirements regarding the precision. Also, differentiation must be made between discharge measurement for flows with steady and non-steady flow conditions, the latter of which encounter problems not completely solved.

The present review aims to introduce the discharge measurement **structures** widely used in Civil Engineering applications. Particular stress is focussed on a rational derivation of the governing flow equations and the resulting expressions for discharge in terms of typical flow quantities and the geometry of the structure. Considerations are restricted to **steady** flow conditions. Furthermore, the present review accounts for discharge of water up from certain minimum limits regarding flow depth and velocity, so that effects of surface tension and viscosity may be overlooked.

In section 2, the general one-dimensional flow equations are presented, and it will be demonstrated that the so-called **critical flow condition** can appear only if additional requirements are satisfied. In particular either the cross-sectional area must have a local minimum, or the bottom geometry is characterized by a local maximum (the case with spatially varied discharge not being considered). Evidently, the first of the respective cases corresponds to so-called discharge

measurement flumes, while the second type is reflected by weirs. Owing to the many situations in which discharge measurement must be evaluated, both flumes and weirs exist in a numerous variety of geometrical types. It is beyond the scope of this review to deal with all of these; therefore, recourse to only the main structures is made. In section 3, devices which show **gradually** varied channel geometry are discussed. These include so-called long-throated flumes (Khafagi-flumes) and hydrofoil weirs. It is found that the classical critical flow theory fits well with observations, and that discharge may be determined on a rational basis.

In section 4, weirs having **rapidly** varying geometry such as thin plate weirs are investigated. It is demonstrated that these may be treated by the same procedure as for gradually varied channel geometry if appropriate modifications of the flow configuration are accounted for. This section deals in particular with thin plate weirs being either contracted or of full width, and V-notch weirs with triangular cross-section.

Section 5 then treats the intermediate structures having **moderately** varied channel geometry such as broad-crested weirs and flumes of the Parshall type. Also discussed are the WES-Standard spillways often found in dam construction and serving for extremely high discharge.

Note that sections 3 to 5 relate to so-called generalized critical flow conditions, by which discharge may be evaluated form a single gauge recording. Particular attention is devoted to the mechanics of flow and not so much to constructive details, which may be consulted in a large number of adapted texbooks [6], [46], Neither, details of how measuring must proceed nor how instrumentation should look are dealt with.

Section 6 applies to the structures considered in the preceeding chapters, but analysis is restricted to the **modular limit**, e.g. the tailwater submergence criteria, by which results may still be regarded as confidential using free flowing conditions. These investigations have a more qualitative character since submerged flow conditions are generally not recommended for discharge measurements.

In section 7, finally, **miscellaneous discharge measurement structures** such as free overfalls, orifices and gates are described. Again, these are not treated in detail owing to the rare application in practice.

All results regarding the evaluation of discharge are presented either by formulae or, if needed, by diagrams. Examples illustrate the computational procedure and facilitate application of the results to problems.

2. CRITICAL FLOW CONDITION IN THE LIGHT OF CLASSICAL HYDRAULICS

2.1. Governing equations

The simplest approach describing flows in open channels smears over variations of the velocity components in the transverse directions and considers the longitudinal axis as the main flow direction. Thus the resulting flow theory is refered to as **one-dimensional.** Evidently, this procedure holds only for flows with a predominant flow direction and must be modified as soon as transverse components become significant.

Let V and h be the average velocity and the average flow depth at a certan location x and at a certain time t. To the lowest order of approximation, uniform velocity and hydrostatic pressure distributions may be assumed for which the de Saint-Venant equations apply. In rectangular channels these may be expressed as [34]

$$\frac{\partial h}{\partial t} + \frac{\partial q}{\partial x} = p \quad , \tag{1}$$

$$\frac{1}{g}\frac{\partial V}{\partial t} + \frac{V}{g}\frac{\partial V}{\partial x} + \frac{\partial h}{\partial x} = S_o - S_f \quad , \tag{2}$$

in which $q=Vh$ is discharge per unit width, p is lateral in- or outflow, g gravitational acceleration, S_o bottom slope and S_f frictional slope. Eqs. (1,2) simplify considerably when restricting considerations to **steady** flow conditions (for which $\partial/\partial t \equiv 0$), the result being

$$q = q_o + \int_x p\,d\bar{x} \quad , \tag{3}$$

$$\frac{d}{dx}\left(z+h+\frac{V^2}{2g}\right) = -S_f \quad . \tag{4}$$

Eqs. (1) and (3) correspond to the continuity equation, while Eqs. (2) and (4) are the momentum equations in the longitudinal direction. Note that $z=z(x)$ describes the channel bottom profile mesured from an arbitrary but fixed reference level, and that $dz/dx=-S_o$.

For flows without lateral in- or outflows, term $p(x)\equiv 0$. This is the usual case in open channel flow except for locations

with junctions, with side-channel spillways (lateral inflow) or distribution channels (lateral outflows), which will not be considered.

Equations (3) and (4) may further be developed by rewriting the continuity equation as

$$Q = VA \qquad (5)$$

in which Q is discharge and A is cross-sectional area. Inserting this into the bracket of (4) results in

$$H = z + h + \frac{Q^2}{2gA^2} \qquad (6)$$

in which H is the energy head. Evidently, this expression states that relative flow energy in a particualr cross-section is composed of the vertical elevation of the channel bottom plus the flow depth plus the velocity head. Inserting this into Eq. (4) then yields

$$\frac{dH}{dx} = -J_f \qquad (7)$$

expressing that the longitudinal change of energy head H equals to the friction slope (note that this in only true for flows without local energy losses, as may appear in bends or sudden enlargements of cross-section). For steady flow conditions, A will be in general a function of both flow depth h and location x, thus $A=A(x,h)$ and $dA/dx=\partial A/\partial x+(\partial A/\partial h)dh/dx$. When differentiating Eq. (6) with respect to x and inserting it into (7), the general **equation of one-dimensional flow profiles** becomes

$$\frac{dh}{dx} = \frac{S_o - S_f + \frac{Q^2}{gA^3}\frac{\partial A}{\partial x}}{1 - \frac{Q^2}{gA^3}\frac{\partial A}{\partial h}} \quad . \qquad (8)$$

This first order differential equation must be solved subject to one boundary condition. Before investigating it in more detail, let us look closely at its main mathematical properties. Extrema of the surface profile occur for $dh/dx=0$, thus

$$S_o - S_f + \frac{Q^2}{gA^3}\frac{\partial A}{\partial x} = 0 \quad , \qquad (9)$$

while vertical tangents are where $dh/dx\to\infty$, thus

$$\frac{Q^2}{gA^3}\frac{\partial A}{\partial h} = 1 \quad , \qquad (10)$$

provided Eqs. (9) and (10) do not hold simultaneously. As will be shown below, it is convenient to express the left hand side of Eq. (10) by

$$F^2 = \frac{Q^2}{gA^3}\frac{\partial A}{\partial h} \quad , \qquad (11)$$

and it is easy to identify F as the **Froude number**. This corresponds to the transition between sub- and supercritical flow states. It yields **minimum** relative energy head for fixed discharge

$$H_* = h + \frac{Q^2}{2gA^2} \qquad (12)$$

in which $H_*=H-z$, or **maximum** discharge Q for fixed energy head H_* [7]. Evidently, the **critical flow condition** is of major importance in open channel flows, since it characterizes the transitional flow state between sub- and supercritical flow, and yields a **unique** depth-discharge relation. Note,however, that for flows with almost parallel streamlines, as assumed above, the condition $dh/dx\to\infty$ violates the basic assumptions. Therefore, and proof can be given for this fact [17], critical flow state can only be achieved when equations (9) and (10) are simultaneously satisfied.

2.2. Location of critical flow

Ensuing developments might be demonstrated for arbitrary cross-sections. However, a straight-forward procedure results for the rectangular cross-section with

$$A = Bh \qquad (13)$$

in which $B=B(x)$ is the channel width.

Critical flow conditions may apply to the transitions from sub- to supercritical as well as from super- to subcritical flow states. However, as already noted, S_f almost vanishes

for the first case, while it becomes significant in the second variant. Moreover, flow in the vicinity of a transition from super- to subcritical flow states is rapidly varied, the result being a so-called hydraulic jump.

It usually consist of two distinctly different flow zones, a more or less fully turbulent lower layer and a separated upper flow zone [18]. This particular phenomenon cannot be adequately described with equations (6) and (7) and will be excluded in what follows.

It can be demonstrated that the above statement concerning the head losses for flows from $F<1$ to $F>1$ can be neglected with respect to other basic assumptions [17]. Therefore, the energy head H in Eq. (6) remains essentially independent of x. Inserting Eq. (13) and differentiating it with respect to x, $()'=d()/dx$, results in

$$H' = z' + h' - \frac{Q^2B'}{gB^3h^2} - \frac{Q^2h'}{gB^2h^3} = 0 \quad . \tag{14}$$

The critical flow condition in the rectangular channel is given by $F=1$, thus

$$\frac{Q^2}{gB^2h^3} = 1 \quad , \tag{15}$$

as is easily evaluated with the aid of Eq. (11). Eq. (14) may be expressed as

$$z' - \frac{Q^2B'}{gB^3h^2} + h'\left(1-\frac{Q^2}{gB^2h^3}\right) = 0 \quad . \tag{16}$$

It is seen that $F=1$ corresponds to the **necessary** critical flow condition, while $z'=Q^2B'/(gB^3h^2)$ represents the **sufficient** critical flow condition. A particular combination of the latter is $z'=0$ and $B'=0$ simultaneously; which is of major practical importance is channels with **variable** discharge Q. The critical flow condition, therefore, may prevail for flows with $F=1$ (according to Eq. (11) for arbitrary cross-sectional shape) at

- a local extremum of the bottom geometry ($z'=0$) and/or
- a local extremum of the cross-sectional area ($B'=0$).

The aforementioned two conditions for the appearance of critical flow do not suffice [21]. Figure 1 shows possible channel geometries with **spatially variable**

cross-sectional area, F(x),
variable bottom geometry, z(x) and
spatially varied discharge Q(x).

Critical flow conditions appear

- for $F=1$, corresponding to a minimum of relative head H_* for fixed discharge, or to a maximum of discharge Q for fixed relative head,
- in a channel with local maximum of the bottom profile ($z'=0$, $z''<0$) and prismatic cross-section A,
- in a channel with a local minimum of channel width ($B'=0$, $B''>0$) and a straight, almost horizontal bottom profile,
- in a channel with spatially varied discharge; critical flow conditions are at the beginning (end) of local outflow (inflow), for which $Q'=0$ and $Q''<0$.

Evidently, these basic types of critical flow locations may be combined with each other, the results then modify accordingly. A typical combination discussed in more detail below are local channel constrictions having a negatively curved bottom geometry. It seems clear that the respective extrema of the

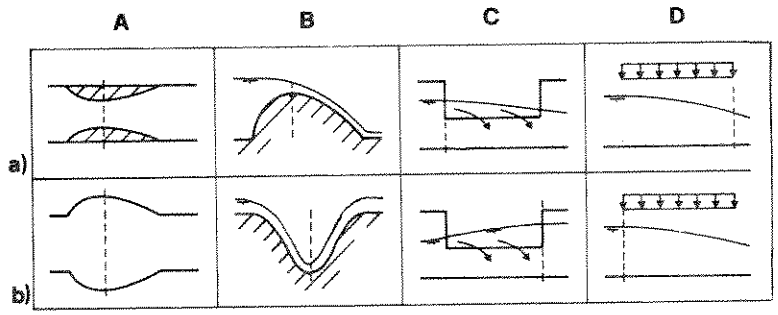

Figure 1 : a) Possible locations of critical points : a) A Venturi channel, B weir, C distribution channel, D side-channel spillway and b) locations where either $z'=0$, $B'=0$ or $Q'=0$, but where sufficient critical conditions are not satisfied.

functions z(x) and B(x) are situated at the same location x, the so-called critical point x_c.

2.3. Head-discharge relation

So far investigations have concerned the definition of the Froude number (see Eq. (11)), and the necessary locations for critical flow conditions have been analysed. This section yields relations between discharge and resulting head (or critical flow depth) for various typical cross-sections. Note that F =1 according to Eq. (11) represents a unique relation between the flow depth h (since A=A(h)) and the discharge Q.

Cross-sections often found in hydraulic practice are shown in figure 2, for which the critical flow condition will be investigated. In particular, the trapezoidal (of which triangular and rectangular profiles are special cases), the U-shaped, and the circular cross-sections will be analysed. Two major aspects are of importance: i) relation between discharge and critical flow depth and ii) relation between discharge and resulting energy head.

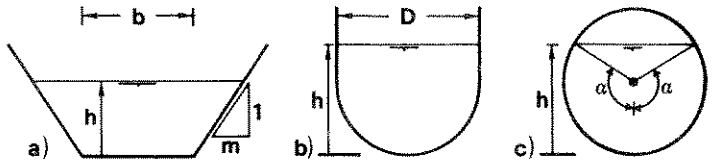

Figure 2 : Geometry of considered cross-sections a) symmetrical trapezoidal, b) U-shaped and c) circular.

Trapezoidal cross-section

A symmetrical trapezoidal cross-section consists of the channel bottom having width b and two side-walls sloped 1:m. The relation between flow depth and the cross-sectional area is

$$A = bh + mh^2 \qquad (17)$$

thus

$$\frac{\partial A}{\partial h} = b + 2mh \quad . \qquad (18)$$

Inserting this into the critical flow condition (10) results in

$$\frac{Q^2(b+2mh)}{g(bh+mh^2)^3} = 1 \quad . \qquad (19)$$

For non-rectangular and non-triangular channels this may further be developed by introducing the scalings

$$Q^{*2} = \frac{m^3Q^2}{gb^5} \quad , \quad y = \frac{mh}{b} \quad , \qquad (20)$$

the result being

$$Q^{*2} = \frac{\{y(1+y)\}^3}{1+2y} \quad . \qquad (21)$$

The relative energy head H with respect to the channel bottom is

$$H = h + \frac{Q^2}{2gA^2} \qquad (22)$$

or, when inserting the non-dimensional parameters (20) and with Y=mH/b

$$Y = y + \frac{Q^{*2}}{2\{y(1+y)\}^2} \quad . \qquad (23)$$

Eqs. (21) and (23) are shown in figure 3; it allows immediate determination of either Q, h or H, provided the geometrical parameters m and b and either Q or h are specified. Note that, upon elimination of Q* in Eqs. (21) and (23),

$$Y = \frac{y(3+5y)}{2(1+2y)} \quad . \qquad (24)$$

This is a relation between critical flow depth and corresponding energy head.

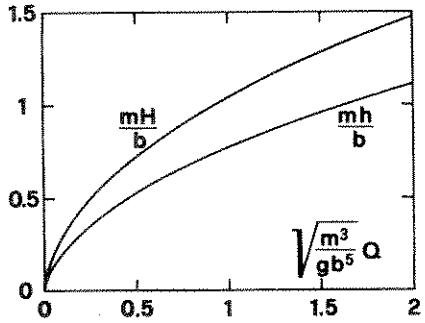

Figure 3 : Relation between discharge Q, critical flow depth h and critical head H in **symmetrical trapezoidal cross-section,** with base width b and slope of lateral side-walls 1:m.

The **rectangular cross-section** may simply be investigated using Eq. (19). By setting m=0, the result becomes

$$h = \{Q^2/(gb^2)\}^{1/3} \qquad (25)$$

and, from Eq. (22),

$$H = 3h/2 \quad , \qquad (26)$$

thus, by elimination of h

$$Q = (\tfrac{2}{3})^{3/2} b\sqrt{gH^3} \quad . \qquad (27)$$

The **triangular cross-section,** in contrast, may be analysed from Eq. (19) by setting b=0, whence

$$h = \{2Q^2/(gm^2)\}^{1/5} \qquad (28)$$

and

$$H = 5h/4 \qquad (29)$$

which is independent of m. Further, it is simple to show that

$$Q = \frac{16}{25} m\sqrt{2gH^5/5} \quad . \qquad (30)$$

The circular cross-section

In the circular profile it is convenient to express the relation between the cross-sectional area and the flow depth with the half central angle α (see figure 2). The result is

$$h = D(1-\cos\alpha)/2 \quad , \qquad (31)$$

$$A = D^2(\alpha-\sin\alpha\cos\alpha)/4 \quad , \qquad (32)$$

from which

$$\partial A/\partial h = D\sin\alpha \quad . \qquad (33)$$

Inserting this into the critical flow condition (10) yields

$$\frac{Q^2}{gD^5} = \frac{(\alpha-\sin\alpha\cos\alpha)^3}{64\sin\alpha} \quad ; \qquad (34)$$

this is expressed as $Q/\sqrt{gD^5}$ as a function of (h/D) using Eq. (31), see figure 4.

The relation between discharge and the critical energy head is computed using Eq. (22)

$$\frac{H}{D} = \frac{h}{D} + \frac{(Q/\sqrt{gD^5})^2}{2(\alpha-\sin\alpha\cos\alpha)^2} \quad ; \qquad (35)$$

upon elimination of the non-dimensional discharge form Eq. (34)

$$\frac{H}{D} = \frac{h}{D} + \frac{\alpha-\sin\alpha\cos\alpha}{8\sin\alpha} \quad . \qquad (36)$$

This is also included in figure 4.

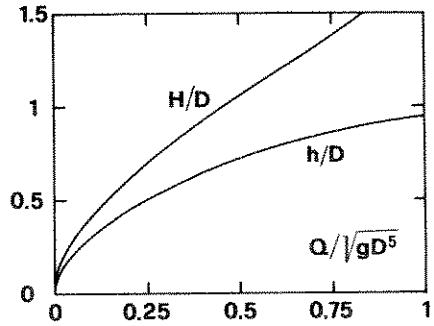

Figure 4 : Relation between relative discharge, critical flow depth and critical head in **partly filled circular profile.**

The U-shaped profile

The U-shaped profile is composed of a circular portion at its lower and a rectangular portion at its upper part. The latter has width D (diameter of the circle, see figure 2) and cross-sectional area

$$A = Dh + D^2(\tfrac{\pi-4}{8}) \quad , \qquad (37)$$

thus

$$\partial A/\partial h = D \quad . \qquad (38)$$

Inserting into the critical flow condition (10) gives

$$\frac{Q^2}{gD^5} = (\frac{h}{D} + \frac{\pi-4}{8})^3 \quad , \quad \frac{h}{D} > \frac{1}{2} \quad . \qquad (39)$$

This is plotted in figure 5, and it is noted that the transition between circular and U-shaped profiles occurs for $Q/\sqrt{gD^5} = (\pi/8)^{3/2} = 0.246$. Evidently, flow will be in the circular portion of the U-shaped profile whenever non-dimensional discharge is lower than this value, and figure 4 must be applied.

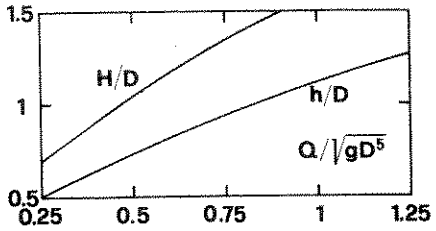

Figure 5 : Relation between non-dimensional discharge, critical flow depth and critical energy head in **U-shaped profile.**

Computation of critical head is straighforward, the result being

$$\frac{H}{D} = \frac{h}{D} + \frac{(Q/\sqrt{gD^5})^2}{2(\frac{h}{D}+\frac{\pi-4}{8})^2} \qquad (40)$$

which, upon inserting Eq. (39), may also be written as

$$\frac{H}{h} = \frac{3h}{2D} + \frac{\pi-4}{16} \quad . \qquad (41)$$

This is also plotted in figure 5. For fixed discharge $Q/\sqrt{gD^5}$, critical flow depth becomes larger in the U-shaped profile than in the circular profile, while this is vice versa regarding the critical energy head H/D. Note that the critical flow depth in circular channels is defined with Eq. (34) for $0<Q/\sqrt{gD^5}<\infty$; from the practical point of view one can set for $h/D\approx 1$ whenever $Q/\sqrt{gD^5}>1.5$.

2.4. Discussion of results

The previous investigation aims at determining the discharge-head relations for critical flow conditions. It has been observed that discharge Q depends solely on the critical flow depth (or on the corresponding critical head H) **and** on the channel geometry **at** the critical point. In particular, the longitudinal shape in the vicinity of the critical cross-section was not necessary to be specified. For a fixed critical cross-section, for instance, it does not matter if it belonged to a local channel constriction or to a local bottom

elevation according to this approach. Evidently, two channels with such particular channel geometries yield different heads H, but these effects are neglected in the elementary approach.

It seems appropriate to discuss in more detail the limitations of the classical critical flow conditon (10) in order to link the various possibilities of critical flow. It is convenient to consider a **prismatic,** rectangular channel having constant discharge q per unit width. Equation (6) then may be written as

$$H = z + h + \frac{q^2}{2gh^2} \quad . \qquad (42)$$

For flows with a transition from sub- to supercritical flow state the energy head H remains essentially constant, thus $H^i\equiv 0$ with $i>1$ as i-th derivative with respect to the longitudinal coordinate x. The first derivatives of Eq. (42) become

$$H' = z'+h'-\frac{q^2h'}{gh^3} \ (=0) \quad , \qquad (43)$$

$$H'' = z''+h''-\frac{q^2h''}{gh^3}+\frac{3q^2h'^2}{gh^4} \ (=0) \quad , \qquad (44)$$

$$H''' = z'''+h'''-\frac{q^2h'''}{gh^3}+\frac{9q^2h'h''}{gh^4}-\frac{12q^2h'^3}{gh^5} \ (=0) \quad . \qquad (45)$$

Inserting into these the critical flow condition $q^2/(gh^3)=1$ results in

$$z' = 0 \quad , \qquad (46)$$

$$z'' + \frac{3h'^2}{h} = 0 \quad , \qquad (47)$$

$$z''' + \frac{9h'h''}{h}-\frac{12h'^3}{h^2} = 0 \quad . \qquad (48)$$

From Eq. (46) it is (again) seen that critical flwo appears at an extremum of the channel bottom geometry; Eq. (47) yields the inclination of the surface profile at the critical point

$$h' = -\sqrt{-hz''/3} \qquad (49)$$

from which it is observed that z" must be negative (corresponding to a local maximum of the channel bottom geometry) in order for h' to be real. The positive root sign in Eq. (49)

may be shown to correspond to the (unreal) transition from super- to subcritical flow states. Inserting Eq. (49) into Eq. (48), the second derivative at the critical point obtains

$$hh'' = -\frac{1}{9}\left(\frac{h^2 z'''}{h'} + 4hz''\right) \quad . \tag{50}$$

It is noted that hh" depends not only on the curvature on the channel bottom **at** the critical point, but that variations of curvature are also to be considered **in the vicinity of the critical point.**

Systematic derivatives of H may be computed in the manner demonstrated above. A general approach is due to Hager [22], and derivatives for arbitrary cross-sections are computed up to the third order. Our essential assumption for the critical flow condition (11) corresponds to an analysis of flow under parallel streamlines (hydrostatic pressure and uniform velocity distributions in the transverse direction). Evidently, this can only be true in a prismatic channel. However, according to Eqs. (49,50), critical flow condition appears only in a channel with variable bottom geometry, (or variable cross-section, or variable discharge). Consequently, streamlines will never be strictly parallel in the vicinity of a critical point.

To the lowest order of approximation, figures 3 to 5 hold for relatively **slightly curved channel geometries** (the resulting flows are said to be shallow). For flows with moderately or even strongly curved streamlines, appropriate modifications must include the channel geometry in the vicinity of the critical point. As an order of approximation, one should apply the above results only for flows in which the absolute values of $h_c'^2$, $h_c h_c''$, $h_c^2 h_c'''/h_c'$ are smaller than 1/2.

3. GRADUALLY VARIED CHANNEL GEOMETRY

3.1. Scope of investigation

This section analyses discharge measurement structures to which the preceeding results apply. These are often found in hydraulic practice and consist either of **weir** type structures, or **flumes** having a local constriction in cross-section, or combinations of the two. It is convenient to analyse the two structures separately and investigate the corresponding main flow characteristics.

3.2. Flumes

A flume is a structure in which the fluid is controlled by a local constriction and discharge can be evaluated from a single flow depth reading. By restricting considerations on structures having **continuous, gradually varied channel geometry,** one may distinghuish between configurations as shown in figure 6. Cross-sections can be arbitrary, but are choosen the simplest in order to avoid design difficulties. The plot refers to rectangular cross-sections; also found are triangular, trapezoidal and U-shaped channel geometries, of which the particular advantages will be discussed.

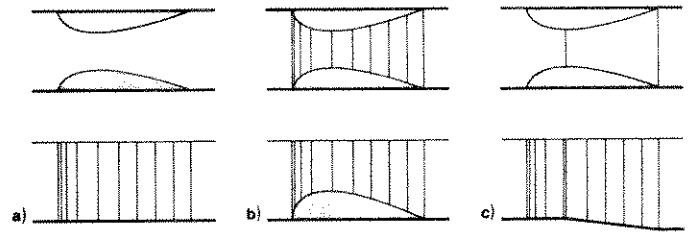

Figure 6 : Typical geometries of continuous Venturi flume; plan view (above) and longitudinal section (below); a) horizontal bottom profile, b) weir bottom type and c) sloped bottom type.

The channel bottom of the flume is either of constant slope (figure 6a), or of weir type with the weir crest at the contracted cross-section (figure 6b) or, finally, consists of a constant up- and downstream slope but having a markedly

sloped flume outlet (figure 6c). The advantage of the configuration a) is its **small loss in head** and its good performance for sediment loaden fluids. These particular advantages are valid only for **small downstream submergence.** All other cases should be designed according to figures 6b) and c).

Rectangular channels

Channels in which discharge is subject to small variation may be designed with a rectanguar cross-section. The head-discharge relation is given by equation (27) in which b corresponds to the contracted channel width and H to the critical energy head at the critical point. Let B>b be the upstream width; neglecting the frictional losses between the upstream zone and the critical point (which is well satisfied when the bottom slope is within 0.1 to 1 %), H remains approximately constant when measured from the channel bottom. Consequently

$$H = h_c + \frac{Q^2}{2gA_c^2} = h_o + \frac{Q^2}{2gA_o^2} \qquad (51)$$

in which indices "c" and "o" refer to the critical and upstream sections, respectively. With $A_o=Bh_o$ and $A_c=bh_c$, this becomes

$$H = h_o + \frac{Q^2}{2gB^2h_o^2} \quad . \qquad (52)$$

Upstream velocity $V_o=Q/(Bh_o)$ is much smaller than the critical velocity. Therefore, it is appropriate to set

$$Q = (\frac{2}{3})^{3/2} b\sqrt{gh_o^3}(1+\frac{Q^2}{2gB^2h_o^3})^{3/2} \approx (\frac{2}{3})^{3/2} b\sqrt{gh_o^3}(1+\frac{3Q^2}{4gB^2h_o^3}) \qquad (53)$$

in which second order terms are omitted. This is a quadratic equation for the unknown Q; its relevant solution is

$$\frac{Q}{b\sqrt{gh_o^3}} = \sqrt{3/2}(\frac{B}{b})^2\{1\pm[1-\frac{8b^2}{9B^2}]^{1/2}\} \approx (\frac{2}{3})^{3/2}\{1+\frac{2b^2}{9B^2}\} \qquad (54)$$

in which series expansions are carried to the second order of approximation. The final result then may be written as

$$Q = (\frac{2}{3})^{3/2} b\sqrt{gh_o^3}\{1+\frac{2b^2}{9B^2}\} \quad . \qquad (55)$$

The right hand side of Eq. (55) contains only measurable quantities (channel geometry rectangular, upstream width, B, width at critical point b, upstream flow depth h_o) and may directly be applied to compute resulting discharge Q. In contrast, Eq. (27) depends on the initially unknown critical energy head.

Figure 7 shows an evaluation of Eq. (55). Also indicated in the figure is the exact correction factor computed from Eq. $(53)_1$, and it is observed that Eq. (55) holds if b/B<0.6 (less than 2% deviation). This accuracy is in general sufficient when regarding the basic assumptions of the present approach, as well as the precision of the flume finishing and, finally, the precision of the gauge reading.

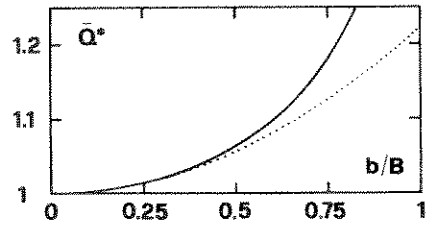

Figure 7 : Effect of upstream velocity head on discharge-upstream flow depth relation; (•••) Eq. (55), (——) Eq.$(53)_1$; $\bar{Q}^*=(2/3)^{3/2}b\sqrt{gh_o^3}$.

Non-rectangular cross-sections

The procedure as presented above is applicable, in principle, to arbitrary cross-sectional geometry. However, computations become unwieldy for non-rectangular flumes and a more suitable method of computation will be developed.

The velocity in the approaching channel is much smaller than the critical velocity (velocity at the critical cross-section). Therefore, it is appropriate (in a first iteration) to set $h_o=H$; inserting H in the corresponding head-discharge relation yields discharge Q_o (which is slightly too small). With known upstream cross-section $A_o(h_o)$, corresponding velocity $V_o=Q_o/A_o$ and resulting head $H_1=h_o+V_o^2/(2g)$ are computed.

The second iterative process starts with H_1 (first iteration) and yields Q_2. This usually corresponds to discharge within the limits of the overall accuracy.

Example

Consider a flume with a rectangular upstream channel having width B=1.5 m; in the vicinity of the critical point, cross-sections alter gradually to a trapezoidal cross-section with width b=0.5 m and m=0.5. What is the resulting discharge-upstream head relation for a channel of constant bottom slope S_o=0.3% and a roughness coefficient K=80 according to the Manning-Strickler formula ? Are there particularities with respect to submerged flow conditions ?

As is seen from figure 8 maximum flow depth in the trapezoidal portion of the cross-section is h_c=1.0 m. With mh/b=1 figure 4 yields $Q\sqrt{m^3/(gb^5)}$=1.64, so that Q=2.57 m^3/s. Further, from figure 4, mH/b=1.33, from which H=1.33 m. It is easy to demonstrate that corresponding upstream flow depth becomes h_o=1.23 m (H_o=1.23+2.57^2/(19.62·1.5^2·1.23^2)=1.33 m).

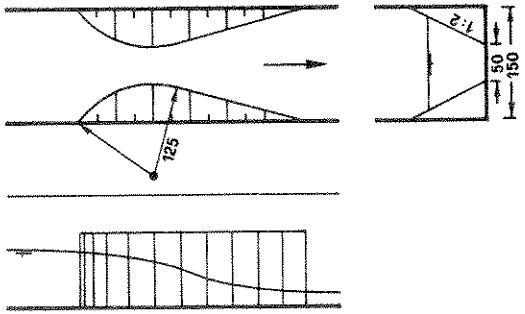

Figure 8 : Plan view, transverse and longitudinal sections of flume with trapezoidal critical cross-section and rectangular approaching channel. Dimensions in (cm).

Let us compute upstream flow depth for Q=1.0 m^3/s. With $\sqrt{m^3/(gb^5)}Q$=0.64, figure 4 yields mH/b=0.82, thus H=0.82 m. The upstream flow depth may be shown to be h_o=0.78 m. Further evaluation of some typical points of the discharge-upstream

flow depth relation allows figure 9 to be drawn. For measured upstream flow depth h_o this plot yields resulting discharge Q. The present, simplified approach should be in a ±5% limit of precision, provided that the radius of curvature is relatively large (in order that no separation from the side-walls occurs, one should choose R>3b/2). Evidently, figure 4 yields discharge only up to Q=2.57 m^3/s. For larger discharge, the composed trapezoidal-rectangular cross-section has to be considered. This yields results in analogy to the U-shaped cross-section.

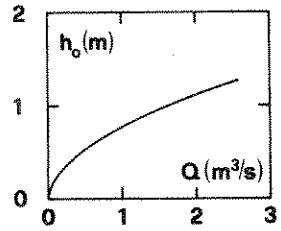

Figure 9 : Discharge-upstream flow depth relation for flume studied in example, see also figure 8.

The asymptotic flow depth in the approaching and the downstream channel is given by the **uniform flow condition.** Using Manning-Strickler's formula

$$Q = K\sqrt{S_o}R_h^{2/3}A \qquad (56)$$

in which K is roughness coefficient, S_o channel bottom slope and R_h hydraulic radius the relation Q(h) can be determined. Figure 10 shows an evaluation for S_o=0.3% and K=80 $m^{1/3}/s$.

For fixed discharge Q figure 4 yields the corresponding critical energy head H. Assuming negligible head losses along the flume, previous computations allow the upstream flow depth h_o to be computed. Further, the (supercritical) downstream flow depth h_u (channel width B=1.5 m) can be computed using Bernoulli's equation. The dotted curve in figure 10 shows the corresponding relation with Q. It is noted that this curve lies always below the uniform flow curve. Finally, with known

flow depth h_u for given discharge Q, it is possible to compute the corresponding Froude number $F_u^2=Q^2/(gB^2h_u^3)$. The sequent flow depth h_s is related to h_u by Belanger's formula

$$h_s = h_u(\sqrt{1+8\ F_u^2}-1)/2 \qquad (57)$$

which allows the determination of the curve $h_s(Q)$, also plotted in figure 10 as dashed curve. Note that this is always higher than the uniform flow depth-discharge curve. Consequently the flume is never submerged from the downstream zone in the present particular case.

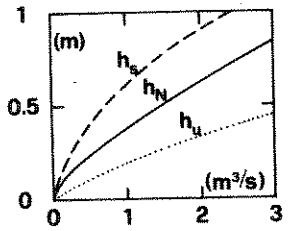

Figure 10 : Evaluation of **downstream** submergence effects on discharge measurement flume; (——) uniform flow curve, (•••) supercritical downstream flow depth and (---) sequent flow depth.

Previous investigations hold for flumes of arbitrary geometry, provided streamlines are nearly parallel (and more or less horizontal). It may be shown that effects of curved and sloped streamlines play only a subordinated role on the discharge characteristics of currently used flumes [22]. Consequently, the present approach will suffice in most practical applications.

3.3. Weirs

Weir -like structures with continuous, slightly curved bottom geometry are rarely found as discharge measurement structures. However, as will be shown below, it is convenient to investigate their most important flow characteristics. The analysis will be restricted to the rectangular, prismatic channel.

Assuming parallel streamlines the fundamental discharge-head relation is given by Eq. (29). Accounting for the transverse variation of the streamline slope and curvature, Eq. (6) is transformed into

$$H = z+h+\frac{Q^2}{2gA^2}\{1+\frac{2hh''-h'^2}{3}+hz''-h'z'-z'^2\} \qquad (58)$$

originally due to Matthew [35] and rederived from first principles by Hager and Hutter [20]. Relations for the transverse pressure and velocity distributions are discussed in detail. Primes in Eq. (58) denote differentiation with respect to the longitudinal coordinate x, and it is observed that Eqs. (58) and (6) become identical for parallel (h"=z"≡0) and horizontal (h'=z'≡0) streamlines. Note that Eq. (58) corresponds only to a first order model. Therefore its validity is restricted on **slightly** sloped and curved streamlines.

Critical flow condition implies dH/dx=0, whence [22]

$$\frac{Q^2}{gA^3}\frac{\partial A}{\partial h} = \{1 + \frac{2hh''-h'^2}{3} + hz'' - \frac{hh''A}{3\partial A/\partial h}\}^{-1} \qquad (59)$$

in which z=0 corresponds to the channel bottom elevation at the critical point. For parallel, horizontal streamlines Eq. (59) simplifies to Eq. (10).

First order derivatives at the critical point have been computed in Eqs. (49) and (50). Inserting these and the third order derivative into Eq. (59) yields [22]

$$Q = (\frac{2}{3})^{3/2}b\sqrt{gH^3}\{1+\frac{22W}{81}\} \qquad (60)$$

in which W=H/R with R as radius of curvature of the channel bottom profile at the critical point. Evidently, our zeroth order solution (27) emerges for H/R→0 (shallow water flow conditions).

It is possible, in principle to extend the above considerations to higher order approximations, but computations then become lengthy. Therefore, recourse to experiments is more favorable, from which the relation

$$Q = (\frac{2}{3})^{3/2} b\sqrt{gH^3}\{1+\frac{22W/81}{1+\frac{3W}{4}}\} \qquad (61)$$

results [22]. This has been derived for parabolic and circular weirs with essentially constant curvature at the weir crest zone. It must be expected from further reaching analysis that effects of third an higher order terms regarding channel bottom geometry influence discharge characteristics for W>1. These particular effects will be discussed in detail below.
Figure 11 shows the evaluation of equation (61) in analogy to figure 7 for flumes, incorporating the (measurable) upstream flow depth h_o instead of H. Note that the upstream weir height is denoted by w, and that

$$H = h_o + \frac{q^2}{2g(h_o+w)^2} \qquad (62)$$

links h_o and H with discharge per unit width q=Q/b. q thus is given by

$$q = C_d(\frac{2}{3})^{3/2}\sqrt{gh_o^3} \qquad (63)$$

in which C_d is the **discharge coefficient.** Evidently, C_d=1 for $h_o/w \to 0$ **and** $h_o/R \to \infty$. Comparing figure 11 with observations if is found that the agreement is (±) 2%, [22].

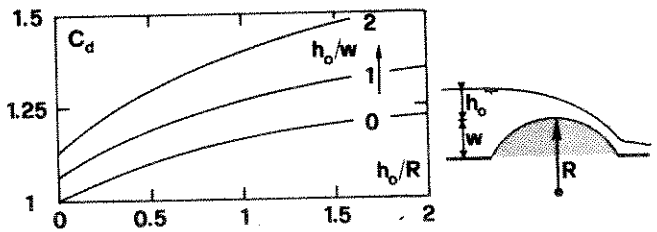

Figure 11 : Discharge coefficient C_d for **circular weirs** in rectangular, prismatic channel as a function of relative weir crest curvature h_o/R and relative weir height h_o/w.

4. RAPIDLY VARIED CHANNEL GEOMETRY

4.1. Description of flow

Completely different in geometry are discharge measurement structures generating rapidly varied flow conditions. Among these, mention might be made of thin plate weirs and orifices. However, the resulting flows may also be computed using the critical flow conditions. In contrast to the gradually varied channel geometry, the jet nappes spring loose from the channel boundary; figure 12 compares flumes and weirs having the two corresponding channel geometries, and it is observed that **separation** from the leading edges occurs. New bounding streamlines divide the potential flow zone from the separation zone in the flume, and water flow from surrounding air for a fully aerated, sharp crested weir. However the qualitative flow behaviour of both gradually and rapidly varied channel geometries is similar, yet the **contraction** of the latter is considerably higher. Therefore, discharge over the first structures is larger than for the second, provided the hydraulic parameters are otherwise identical.

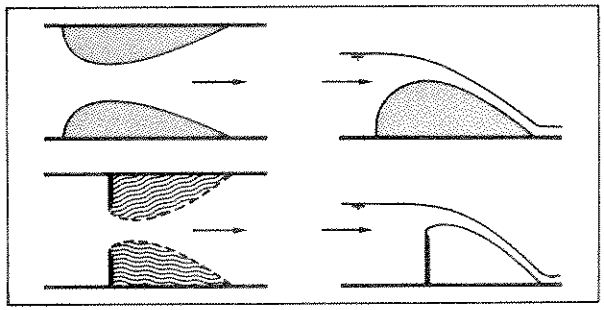

Figure 12 : Flow in flume (left) and over a weir (right) with gradually varied (top) and rapidly varied (bottom) channel geometry. Flows in rapidly varied channel geometry separate from the bounding channel geometry.

The previously discussed discharge-head relations remain valid if the width of the contracted cross-section and the corresponding streamline curvatures are known. Owing to the

significant streamline curvature at the critical point (now at the contracted cross-section with respect to the bounding streamlines) the analysis becomes involved. Consequently, recourse to observations is a useful approach.

Ensuing considerations are restricted to weir flow. The corresponding flow characteristics in flumes [4] are of limited practical application. Further informations are given by Vallentine [57], Ramamurthy et al. [44] and Hager and Dupraz [23].

4.2. Rectangular sharp crested weir

Owing to the simple geometry the **thin plate weir** in rectangular channels is one of the oldest discharge measurement structure. A first systematic investigation into the overall flow behaviour is due to Poleny in the 18th century, the result being the discharge-head relation

$$q = \frac{2}{3}\mu\sqrt{2g}h^{3} \qquad (64)$$

in which μ is the corresponding discharge coefficient. Assuming nearly parallel streamlines results in $\mu=1/\sqrt{3}=0.577$. Observations of Poleni indicated that $\mu=0.64$, and it was only Boussinesq [7], who gave physical reasons for the deviation of some 10%. In an elegant approach, it is shown that the **streamline curvature** plays the significant role in flows over thin plate weirs, and that the augmentation of the discharge coefficient must primarily be attributed to this effect.

The result of Boussinesq may be expressed as [13]

$$\mu = 0.651(1-0.391\frac{i}{\pi}) \qquad (65)$$

in which i is the angle of the thin plate weir with respect to the vertical, see figure 13. Eq. (65) is only valid for $w/h \gg 1$ w being the weir height.

In practice, the usual case consists of a **vertical thin plate weir** with width b equal to up- and downstream channel widths. Detailed and precise observations of several investigators lead to the formulae given in Table I [17].

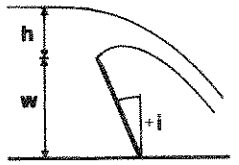

Figure 13 : Sharp crested, full-width rectangular weir with deviated angle i from the vertical. The lower jet surface is fully aerated.

All **discharge coefficients** except that of Kindsvater and Carter contain three different terms : i) a constant having value of roughly 0.610, ii) a term accounting for surface tension effects being proportional to 1/h (h in [m]); Sarginson [50], in a semi-empirical approach derives μ in terms of the Weber number $We=\gamma h^2/\sigma$ in which γ is specific weight of the fluid and σ surface tension and iii) a term accounting for the velocity of approach, involving the geometrical ratio h/w.

Bazin (1888)	$\mu = 0.6075(1+\frac{0.074}{h})(1+0.55(\frac{h}{h+w})^2)$	(66)
Rehbock (1913)	$\mu = 0.6050(1+\frac{0.0019}{h})(1+0.138\frac{h}{w})$	(67)
SIA (1924)	$\mu = 0.6150(1+\frac{0.001}{h+0.0016})(1+0.5(\frac{h}{h+w})^2)$	(68)
Kindsvater, Carter (1957)	$\mu = 0.6020(1+0.125\frac{h}{w})$	(69)
Sarginson (1972)	$\mu = 0.6130(1+\frac{2.33}{We}+0.122\frac{h}{w})$	(70)

Table 1 : Discharge coefficients μ according to Eq. (64) for thin plate, fully aerated, prismatic rectangular weirs; all lengths in (m), for details see text.

Kindsvater and Carter's discharge coefficient is related to the discharge formula

$$q = \mu\sqrt{g}h_e^{3} \quad , \quad h_e = h+0.9(mm) \qquad (71)$$

by which surface tension effects are included.

A widely accepted relation for the discharge coefficient is the second version of Rehbock's formula [49] published in 1929

$$q = 0.4023\sqrt{2g}(h+0.0011)^{3}\{1+0.135\frac{h}{w}\} \qquad (72)$$

in which h is to be inserted in (m) and the ratio h/w should be smaller than 0.5. The precision is between 0.1 to 0.2%, provided that the thin plate weir geometry is properly designed and the nappe **fully aerated.** Figure 14 gives details of the weir crest finishing for arbitrary thin plate weirs.

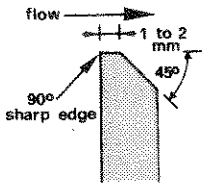

Figure 14 : Details of sharp-crested geometry for thin plate weirs.

A more general case of the aforementioned full-width aerated weir (weir width b equal to channel width) is the so-called **contracted thin plate weir,** having width b and channel width B>b, see figure 15. Extensive tests of the discharge coefficient is due to SIA [53]; their result may be expressed as

$$\mu = 0.578\{1+0.064\beta^{2}+\frac{6.25-5.19\beta^{2}}{1000(h+0.016)}\}\{1+0.5\beta^{4}(\frac{h}{h+w})^{2}\} \quad , \qquad (73)$$

in which $\beta=b/B<1$ but $\beta>0.3$. This relation for μ according to Eq. (64) consists of four terms, one having again the basic value of about 0.6, a second accounting for effects of the approach velocity, a third for effects of surface tension (insert h in m), and a forth for the effect of β on discharge q. Note that Eqs. (73) and (68) become identical for full-width weirs, $\beta=1$.

Other formulae have been proposed by Kindsvater and Carter [29] and Bazin [3], but differences between the respective

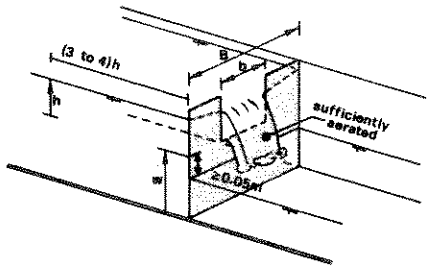

Figure 15 : Rectangular sharp-crested weir with contracted weir width b in a rectangular channel of width B.

discharges are normally insignificant. Note that the following basic requirements must be fulfilled when applying such formulae; i) B-b>4h, ii) h/w<0.5, iii) h/b>0.5, iv) w>0.30 m, v) $0.025/\beta>h>0.80$ m, vi) b>0.30 m. Violating any of these requirements may lead to serious errors in discharge.

4.3. V-notch sharp-crested weir

A V-shaped notch in a vertical thin plate placed perpendicular to the sides and bottom of a straight, normally rectangular channel is refered to as a **V-notch** sharp-crested **weir.** It is one of the most precise discharge measurement devices suitable for a wide range of discharge.

As a head-discharge relation, one uses the modified equation (30)

$$Q = \frac{8\mu}{15}\cdot\tan(\theta/2)\sqrt{2g}h_e^{\frac{5}{2}} \quad , \quad h_e = h_o+1mm \qquad (74)$$

in which $m=\tan(\theta/2)$ and $h_o\approx H$ is upstream flow depth. This relation is accredited to Thomson, and V-notch weirs are also denoted as Thomson-weirs. According to Eq. (30) the discharge coefficient $\mu=6/5\sqrt{5}\approx0.537$. By dimensional analysis, it may be demonstrated that $\mu=\mu(h/w,w/B,\theta)$ in which B is upstream channel width [6]. For **fully contracted V-notch weirs** ($h/w<0.4$, $w/B<0.2$) one has solely $\mu=\mu(\theta)$. Table II gives the corresponding relation for typical values of θ, and it is noted that $\mu(\theta=70^{o})=\mu_{min}=0.577$.

θ (°)	20	40	60	80	90	100
μ	0.595	0.582	0.577	0.577	0.578	0.580

Table II : Discharge coefficients μ according to Eq. (74) as a function of the angle θ.

Partially contracted V-notch weirs underlie the geometrical conditions $h/w<1.2$, $h/B<0.4$, $0.05<h<0.60$ m, $w>0.10$ m and $B>0.60$ m. Both, approach velocity and channel width effects then become important. Figure 16 shows the resulting discharge coefficient as a function of h/w and w/B for the 90° V-notch weir [6]. It is to be noted that the upstream channel should be rectangular or of nearly rectangular shape.

Usually, one will choose the angle θ as a fraction of θ=90°. The "Association française de normalisation" [6] provides Tables for discharge in (ℓ/s) in terms of the head h_o in (mm) for V-notch weirs having 90°/4 (θ=28.4°), 90°/2 (θ=53.8°) and 90°/1 (θ=90°). These allow an accurate determination of relatively low discharge ($0.21<Q<124$ ℓ/s) with accuracy better than 1%.

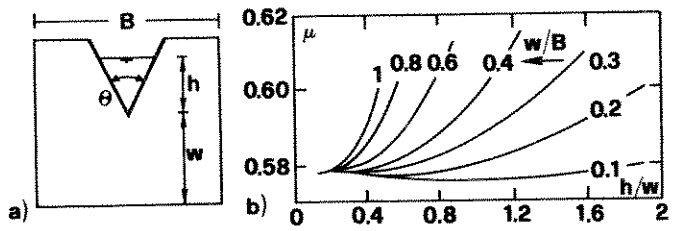

Figure 16 : V-notch sharp-crested weir, a) definition of channel geometry, b) discharge coefficient μ for partially contracted flow conditions as a function of h/w and w/B [6].

Further informations on V-notch sharp-crested weirs are due to Lenz [33] who investigates effects of viscosity and surface tension on the discharge coefficient. Ramponi [45] analyses

the effects of the upstream channel on the flow characteristics, and De Coursey and Blanchard [10] study the flow characteristics over large triangular weirs.

Further types of sharp-crested weirs are the **Cipoletti-weir** having trapezoidal cross-section [36], the **circular sharp-crested weir** and so-called **proportional weirs.** The latter's shape is such that the relation between discharge and upstream head is linear. All of these discharge measurement structures are rarely applied and will not be described here. Reference is made to more detailed investigations such as these of Bos [6], or Rao [46]. Finally, Gentilini [15] summarizes the knowledge on weir flow with sharp weir crests for various weir types.

5 . MODERATELY VARIED CHANNEL GEOMETRY

5.1. Introduction

Discharge measurement structures with moderately varied channel geometry are intermediate between gradually and rapidly varied channel geometry. Applications include weirs and flumes, and we will discuss both of these flow types. The flow at the critical cross-section is **partly separated** from the channel bottom and/or the side walls. From the hydraulic point of view, the separation complicates the prediction of the discharge-head relation. However, the geometry of these structures is simple (normally of only a polygonial system of boundaries). Consider, for instance, the **broad-crested weir** in a prismatic channel having weir height w and upstream flow depth h. Its counterpart is the airfoil-shaped weir having a relatively complex channel bottom geometry z(x) but leading to non-separated flow conditions (see figure 17). Evidently it is simpler to construct the broad-crested weir but it will be more difficult to predict discharge Q from upstream flow depth reading.

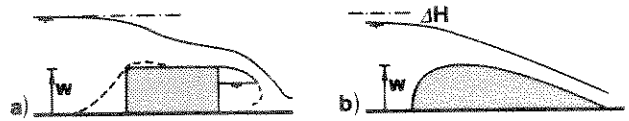

Figure 17 : Weirs of equal height w in a rectangular channel having identical flow conditions, a) broad-crested weir with separation zones at the upstream leading edge and b) airfoil weir having gradually varied bottom geometry and no separation zones. Under equal discharge, the upstream flow depth is higher (Δh) in case a) than in b).

5.2. Broad-crested weirs

Consider a rectangular prismatic channel in which a square stone of length L, width b and height w is placed (see figure 18). Evidently, flow cannot follow this bottom geometry but will create two dead-water zones, one of which is located at the upstream side of the broad-crested weirs having over-

pressure when compared with the hydrostatic pressure distribution, while the second is at the leading upstream edge of the weir, the resulting separation zone having underpressure when compared with the hydrostatic pressure distribution. A third **separation zone**, not discussed in connection with critical flow conditions, is located at the downstream end of the weir.

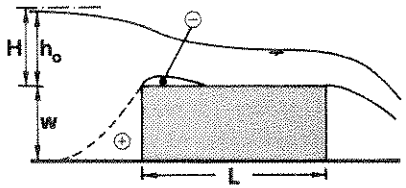

Figure 18 : Flow pattern of broad-crested weir in prismatic, rectangular channel. Note that leading upstream edge is sharp, and that ⊕ and ⊖ denote zones of separation with positive and negative pressure defects with respect to the hydrostatic pressure distribution, respectively.

In the past, a large number of researchers have refered flow over broad-crested weirs as a perfect example in which the classical theory of critical flow may be applied. The supporting argument was that streamlines are nearly parallel along the weir crest zone, provided the weir length, L, is sufficiently long. It is seen from figure 18, however, that streamlines are considerably sloped and curved at the critical flow zone (zone at which the separation thickness has a maximum). Therefore, the above argument becomes invalid, and discharge characteristics must be sought subject to the effective flow behaviour [37].

Several investigators have attempted to describe the head-discharge relation for broad-crested weirs [12], [27], [58], but no solution accounts for the relatively complex flow phenomena. Therefore, recourse to experiments is necessary. From Eq. (27) it is reasonable to express discharge as

$$Q = C_d b\sqrt{2gH^3} \qquad (75)$$

in which C_d is related **discharge coefficient.** For strictly parallel streamlines $C_d=(2/3)^{3/2}=0.385$.

By dimensional analysis, Rao and Muralidhar [47] find that C_d must be a function of the relative approaching flow depths h_o/L and h_o/w. However, as is indicated by experiments, the effect of the latter parameter is usually insignificant, such that $C_d=C_d(h_o/L)$ alone. Evidently, parameter h_o/w accounts for the upstream velocity head by which h_o and $H=h_o+Q^2/(2gb^2(h_o+w)^2)$ are related. Figure 19 shows the functional relation for C_d according to Rao and Muralidhar's data. Also plotted are results of Bazin [3], USGS [56], and Keutner [27]. It is observed that Rao and Muralidhar's curve lies considerably above all others, and that these latter may be expressed as [17]

$$C_d = 0.42\{1-\frac{2}{9(1+\zeta^4)}\} \quad , \quad \zeta = H/L \qquad (76)$$

which is plotted as solid curve in figure 19.

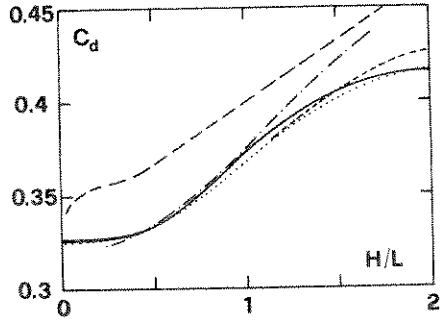

Figure 19 : Discharge coefficient C_d according to Eq. (75) for broad-crested rectangular weir; observations according to (– –) Rao and Muralidhar [47], (•••) USGS [56], (-•-) Bazin [3], (---) Keutner [27] and (——) Eq. (76).

Rao and Muralidhar [47] distinguish between four different flow types over a broad-crested weir, depending on the relative length of the weir crest h_o/L, see figure 20. Weirs with $0<h_o/L<0.1$ are refered to as very long weirs for which standing surface undulations are observed. In region 2 ($0.1<h_o/L<0.35$) the flow is over truely broad-crested weirs and

the streamlines are nearly parallel at the downstream zone of the weir. Weirs are narrow-crested for $0.35<h_o/L<1.5$ to 1.9. Finally, sharp-crested weirs as discussed in section 4 result for $h_o/L>1.5$ to 1.9 [47]. Inserting $\zeta \to \infty$ in equation (76) yields $C_d=0.42=2\mu/3$, which is an average value found in Table I.

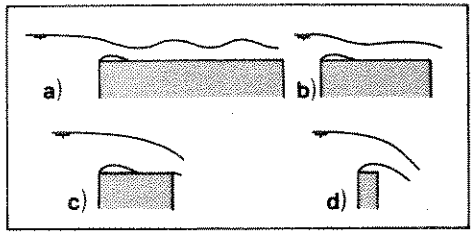

Figure 20 : Typical surface profiles over broad-crested rectangular weirs as a function of relative weir crest length h_o/L: a) very long weir, $0<h_o/L<0.1$, b) broad-crested weir, $0.1<h_o/L<0.35$, c) narrow-crested weir, $0.35<h_o/L<1.5$ to 1.9 and d) sharp-crested weir for $h_o/L>1.5$ to 1.9.

In constrast to the above described broad-crested weir with sharp upstream corner, the **streamlined broad-crested weir** is rounded with radius of curvature $R>0$ at the upstream corner, see figure 21. This weir type is extensively described by Harrison [26] and Hall [25]. Yet, there have not been accomplished systematic observations which allow an accurate prediction of the discharge coefficient.

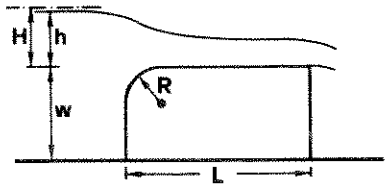

Figure 21 : Broad-crested weir with rounded upstream corner.

Let R^* be the radius of bottom curvature for which the bottom streamline no longuer separates from the weir surface. Evidently, weirs with $R>R^*$ may be computed using the results obtained in section 3, while the others are intermediate cases between these and broad-crested weirs with $R=0$. From Keutner's observations [27] it may be noted that R^* is of order h_o.

The effect of the upstream slope i on discharge characteristics has been investigated by Bretschneider [8]. His observations include slopes 1:1, 1:1.5 and 1:2 but only small relative weir length $h_o/L<0.25$. Discharge coefficients C_d are plotted in figure 22, and it is found that the effect of the slope i on the discharge coefficient is nearly insignificant. Average values are $C_d(i=1:1)=0.346$, C_d $(i=1:1.5)=$ 0.362, and $C_d(i=1:2)=0.354$. Also included as open circles and squares are data for which effects of surface tension become significant; finally, equation (76) has been plotted as solid curve. It is observed that the discharge coefficient may slightly be augmented (some 5 to 10%) when the upstream weir bottom is sloped instead of vertical.

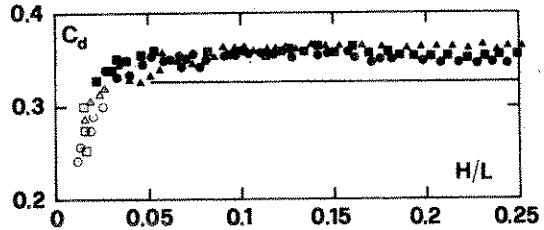

Figure 22 : Discharge coefficient C_d with respect to Eq. (75) for upstream sloped, broad-crested weirs in prismatic, rectangular channel according to Bretschneider [8] for (●) i=1:1, (▲) i=1:1.5 and (■) i=1:2; open signs denote data in which effects of surface tension becomes significant, and the solid curve corresponds to Eq. (76).

5.3. The WES-Standard spillway

Thin plate weirs, being one of the most precise discharge measurement structure suffer from the fact of their static stability. Whenever discharge is larger than several m^3/s, preferably weirs having sufficiently large longitudinal extension are choosen. The simplest of such weirs, the broad-crested weir, exhibits distinct separation zones; further, the discharge coefficient is relatively small. Therefore, the weirs crest zone must be designed such that these two major disadvantages are removed.

The simplest idea regarding the pressure distribution on the spillway bottom is to copy the lower jet surface of a fully aerated **thin plate weir,** see figure 23. Detailed observation of the lower jet zone is due to Scimeni [52]; it was found that the largest vertical and horizontal displacement from the weir crest is 0.11H and 0.25H, respectively, in which H is the head on the vertical thin plate weir. Figure 23b) shows the equivalent bottom geometry to a vertical thin plate weir for which the origin is situated at the weir crest. Evidently, flow characteristics will be identical if $\bar{H}$=0.89H; in particular, the bottom pressure on the spillway then is atmospheric.

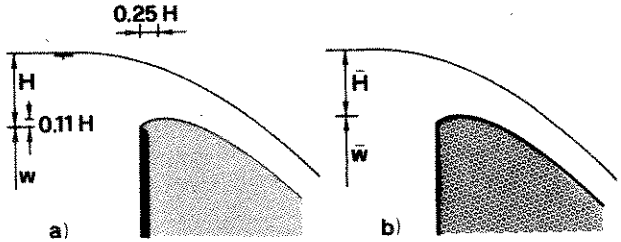

Figure 23 : a) vertical thin plate weir with fully aerated lower jet surface and b) equivalent spillway with corresponding head $\bar{H}$<H but $\bar{w}$>w.

Spillways of which the bottom geometry corresponds to the lower jet surface of a fully aerated thin plate weir are refered to as **standard-shaped weir.** The energy head, for which the two weirs become identical regarding the flow characteristics, is refered to as **design head** H_D.

Let (x,z)=(0,0) be the origin of a Cartesian coordinate system at the weir crest of the **standard spillway.** The lower jet surface (or the bottom geometry of the standard spillway) may then be expressed by the non-dimensional parameters

$$X = x/H_D \quad , \quad Z = z/H_D \tag{77}$$

as

$$Z = \frac{1}{2}X^{1.85} \quad , \quad X > 0 \tag{78}$$

and

$$Z = 0.724(X+0.27)^{1.85} - 0.432(X+0.27)^{0.625} + 0.126 \quad , \quad -0.27 > X > 0 \tag{79}$$

in which Z is measured vertically downwards and X horizontally in the flow direction. Eq. (78) is due to Scimeni [52], while Eq. (79) has been proposed by the US Army Engineers [56]. Figure 24 shows the non-dimensional bottom geometry of a Standard spillway according to Eqs. (78) an (79).

The discharge characteristics of Standard spillways may be investigated using Eq. (75) in which H=$\bar{H}$ is the head on the spillway measured from its crest. In what follows, the bars on quantities refering to the standard spillway are dropped. Figure 25 is a plot of observed discharge coefficients according to Schirmer et al. [51] from which $C_d(H/H_D=1)$=0.494. Evidently, $C_d(H/H_D<1)<0.494$, while C_d is larger for higher relative head H/H_D.

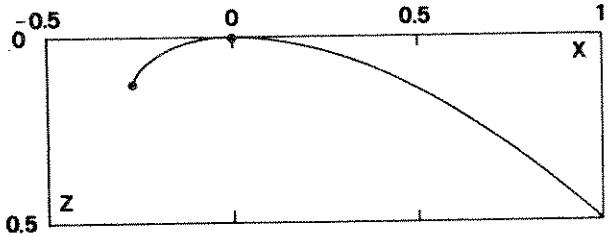

Figure 24 : Non-dimensional bottom geometry Z(X) of a Standard spillway.

For $H/H_D \to 0$, the asymptotic value $C_d = 2/(3\sqrt{3})$ is found as predicted in Eq. (27), if effects of surface tension are excluded.

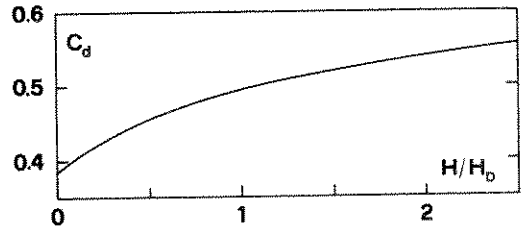

Figure 25 : Discharge coefficient C_d according to Eq. (75) for standard spillways as a function of non-dimensional head H/H_D.

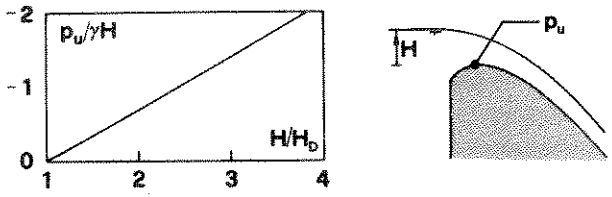

Figure 26 : Non-dimensional pressure $p_u/(\gamma H)$ at he crest of a Standard spillway as a function of relative head H/H_D.

Spillway crest pressure p_u may be determined using Bernoulli's equation. It is observed from figure 26, in which the non-dimensional spillway crest pressure $p_u/(\gamma H)$ is plotted as a function of relative head H/H_D that it decreases almost linearly with increasing relative head H/H_D. This significant low pressure may be of serious danger

- if flow is not completely plane, air can entrain from the side-walls of the spillway (at the piers, for instance) and create **separated flow conditions,** for which the bottom pressure becomes atmospheric. The result is a rapid augmentation of head.

- even for completely plane flow conditions, since the under-pressure can decrease so far that vapor pressure is reached. As a result, water boils locally and, when flowing back to zones of nearly atmospheric pressure, the vapor bubbles collapse instantaneously. This effect is refered to as **cavitation,** see also [30]. Abecassis [1] gives values of the **absolute** head H, for which cavitation danger begins (see figure 27).

Note that cavitation does **not** only depend on the ratio H/H_D but also on the **absolute** head H (m). Therefore, it is possible to design Standard spillways with H/H_D=4, for instance, if H remains lower than H=0.4 m, but H/H_D should be smaller than 1.4 from figure 27, if H is as high as H=20 m.

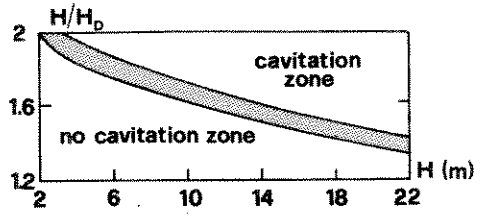

Figure 27 : Zones of cavitation and without cavitation as a function of relative and absolute head in meters according to Abecassis [1].

Lemos provides an extensive description of the longitudinal bottom pressure, the surface profiles, and the minimum pressures at the spillway crest zone for various upstream weir shapes [32].

5.4. Flumes

Flumes may either be long-throated or throatless, the first of which have been discussed in section 3. In contrast to these, **throat less flumes** with broken plane transitions yield separation zones as is shown in figure 28. A particular structure is the **Parshall flume,** which consists of a converging section with a level floor, a throat section with a downward sloping floor, and a diverging section with an upward sloping floor.

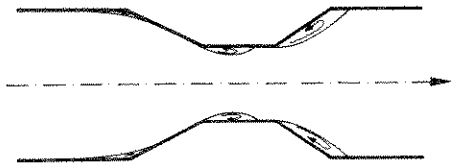

Figure 28 : Flume with broken plane transitions and resulting separation zones (schematically).

In deviation from the general rule for long-throated flumes, where the upstream head must be measured in the approach channel, Parshall flumes are calibrated against a piezometric head h_a, measured at a prescribed location in the converging section. The "downstream" piezometric head h_b is measure in the throat section, see figure 29.

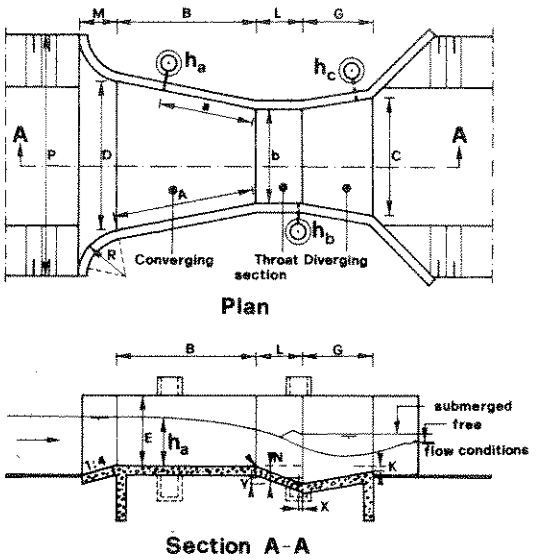

Figure 29 : Parshall flume dimensions.

Parshall flumes were developed in various sizes, the dimensions of which are given in tables [6]. Care must be taken to construct the flumes **exactly** in accordance with the structural dimensions given for each of the 22 possible flumes, as they are not hydraulic scale models of each other. The range of discharge is between zero to 90 m^3/s. Relations between discharge and head h_a for free flow conditions, and additionally with h_b for submerged flow conditions are listed in tables [6]. The accuracy of discharge measurement may be expected within 3 %.

Recently, a new type of moderately varied flume geometry has been proposed [24]. Instead of positioning the lateral contraction elements at either side of the channel walls, they are inverted and inserted in the center of the flume. For rectangular channels, the result then is a circular **cylinder,** while circular **cones** result for trapezoidal channels. This modified flume shape has certain advantages over the conventional configuration; in particular, such an element may easily be inserted in any channel of well defined shape (mobile discharge measurement structure) and is precise regarding the finishing.

6. Modular limits

Results derived in chapters 3 to 6 relate to **free-flowing conditions,** for which discharge is prescribed only by the upstream zone. Evidently, this procedure must be modified whenever the downstream level rises such that flow conditions are **submerged** at the critical point. Two particular questions arise in connection with these flow conditions :

- What is the limiting downstream level for which flow conditions are still free ?
- How must the discharge-upstream head relation be modified when downstream level has risen above the limiting level ?

In context with discharge measurement structures the second question is rather insignificant. One will usually position the structure such that either submerged flow conditions do not appear, or that precision of discharge measurement is not accurate for such flow conditions. More interesting are the downstream limit levels which assure a still accurate determination of discharge using free flowing approach.

Figure 30 shows different stages of **submergence** in weir flow; the corresponding phenomena appear for all other structures discussed. For low downstream submergence a standing wave train may be observed at the downstream zone of the weir, see figure 30b), in which the amplitudes and wave lengths decrease for moderate downstream submergence, see figure 30c). For high dowstream submergence, the surface profile becomes almost horizontal. Also plotted in figure 30 is the bounding streamline of the flow, which separates the main flow from the separation zone situated below it. Note that this curve becomes the flatter and the less curved, the higher the downstream submergence is.

The preceeding description may be analysed using Eqs. (42) to (45). Locally, one may still suppose that the energy head remains constant, thus $H'=H''=H^{i}\equiv 0$. Let $z'=0$ denote a point of the bottom streamline at which $z=0$ (reference level), thus $H_*=H-z$ and $H_*=h'\{1-q^2/(gh^3)\}$ from Eq. (43). Evidently $H'=H''=0$

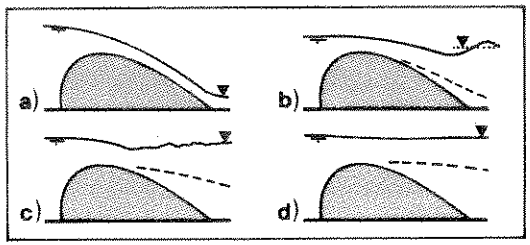

Figure 30 : Different typical stages of submergence for weir flow, a) free overflow, b) low submergence with standing waves, c) moderate submergence with small standing wave train and d) high submergence without waves. Dashed curves correspond to the bounding streamlines which divide the separation zone from the main flow zone.

at the point where $z'=0$. Therefore, the above condition is fulfilled either for $q^2=gh^3$ (critical flow condition) or for $h'=0$ ("pseudo-critical" flow condition). As has been demonstrated in section 2, the latter can only be fulfilled provided $q^2 \neq gh^3$. Inserting the condition $h'=0$ into Eqs. (44) and (45) results in

$$h'' = - \frac{z''}{1- F^2} \quad , \tag{80}$$

and

$$h''' = - \frac{z'''}{1- F^2} \tag{81}$$

in which the conditions $H^i=0$ have been accounted for. A local solution of the surface profile then may be expressed by the Taylor series

$$h(x) = h_i - \frac{z''x^2}{2(1- F^2)} - \frac{z'''x^3}{6(1- F^2)} + O(x^4) \tag{82}$$

in which $h_i=h(x=0)$ is the initial flow depth and z^i are the derivatives of the separating bottom streamline at the origin $x=0$. Submerged flows are characterised by $F<1$ (thoroughly subcritical flow conditions). Further, as is seen from figure 30, the separating streamlines are negatively curved, $z''<0$, and $|z''(x)|$ decreases with increasing x, thus $z'''>0$. If

$a=|z''|/\{2(1- F^2)\}$ and $b=|z'''|/\{6(1- F^2)\}$, both of which are known values for given discharge and weir geometry, Eq. (82) results in

$$h(x) = h_i + ax^2 - bx^3 + O(x^4) \quad . \tag{83}$$

This relation indicates that the free surface profile is positively curved, but that the downstream level must be lower than the corresponding level at the upstream zone. This is the situation as plotted in figures 30b) to d). Further, it is simple to demonstrate with Eq. (12) that this case does not correspond to a minimum energy head $H*(h)$ but yields only a local minimum $H=H(x)$.

The above considerations suggest application of the results as presented in sections 3 to 5. However, this approach regarding the determination of the separating streamline $z(x)$ has failed until to date. By contrast it has been shown that the "pseudo-critical" flow condition does not yield a minimum energy head for fixed discharge, and that one gauge reading does not suffice for the evaluation of discharge. In order to apply the results of free flowing conditions in the present case, it is convenient to define the discharge-head relations as

$$Q_s = \phi \cdot Q_f \quad , \tag{84}$$

in which indices "s" and "f" refer to submerged and free flow conditions and ϕ is a **submergence factor.** ϕ has the range $0 \leq \phi \leq 1$, and depends on the ratio of H_u/H_o and on the channel geometry. Note that H_u is measured from the same reference level as H_o (upstream head under free or submerged flow conditions), and that the respective range is $0 \leq H_u/H_o \leq 1$. Evidently, $\phi(H_u/H_o=0)=1$, while $\phi(H_u/H_o=1)=0$ (see figure 31).

Figure 31 : Notation for submerged flwo conditions. All parameters are measured vertically from the spillway crest.

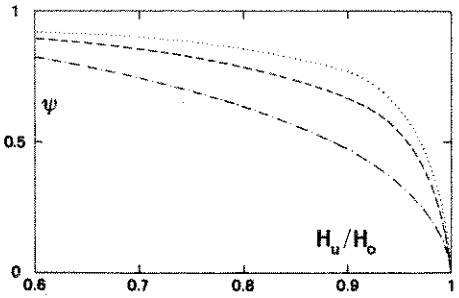

Figure 32 : Submergence factor ϕ according to Eq. (84) for various discharge measurement structures, (•••) broad-crested weir [6], (-•-) sharp-crested thin plate weir [17], (---) cylindrical weir [6].

Consequently, ϕ may be expressed as

$$\phi = \{1 - v^a\}^b \qquad (85)$$

in which $v=H_u/H_o$ and a,b are coefficients to be determined experimentally. Figure 32 shows selected relations $\phi(v)$; for sharp-crested weirs, for instance, Hager [17] determines a=2 and b=1/2 for arbitrary weir geometry according to observations of Abou-Seida [2]. For cylindrical weirs in rectangular channels, one might set approximately a=3 and b=1/3; finally, for broad-crested weirs of sufficient length L, a=4 while b=1/4, such that Eq. (85) can be simplified to

$$\phi = \{1 - v^a\}^{1/a} \quad , \quad a > 1 \quad . \qquad (86)$$

This approximation is independent of the geometry of the structure; the coefficient "a" must be determined experimentally. Note that the donwstream submergence starts (theoretically) as soon as $H_u>0$, but that it influences the discharge-head relation significantly for $\phi<0.95$, say. The corresponding non-dimensional head ratio v* then becomes v*(a=2)=0.3, v*(a=3)=0.53, v*(a=4)=0.65. Generally, one may state that the discharge-head relation remains nearly unaffected provided that the downstream submergence $v=H_u/H_o$ is below 50 %. For high precision, however, one should never employ submerged flow conditions. Therefore, it is recommmended (even for thin

plate weirs) that the downstream level be at least 5 cm below the weir crest. This security distance guarantees an accurate determination of the discharge and allows for a sufficient aeration of the nappe.

7. MISCELLANEOUS STRUCTURES

Besides weirs and flumes, there are other structures often found in hydraulic practice, with which discharge measurement may be performed. However, only the first devices are based on the critical flow condition, while the latter use either the uniform flow condition, or particular relations between some flow depth and discharge.

7.1 Free overfall

Figure 33 shows a so-called **free overfall** which corresponds to a channel with constant positive slope at the upstream zone, and a sudden drop at the brink section. The downstream tailwater depth should be at least at a distance h_o below the brink and the lower jet surface must be sufficiently aerated in order to guarantee atmospheric pressure conditions.

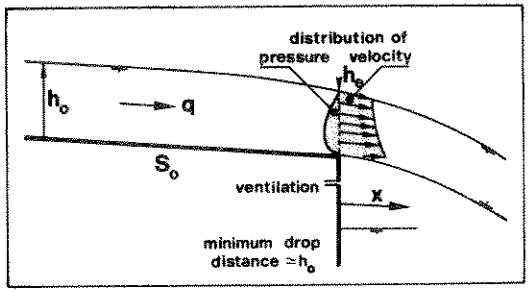

Figure 33 : Flow characteristics over free overfall; typical distributions of pressure and velocity at the brink section.

Let S_o be the constant bottom slope, K=1/n the roughness coefficient according to the Manning Strickler formula, b the constant width of the rectangular channel and h_o the asymptotic upstream flow depth. Discharge per unit width then may be evaluated using the uniform flow condition (56)

$$q = K\sqrt{S_o}\,h_o^{5/3}/(1+2h_o/b)^{2/3} \quad . \qquad (87)$$

Evidently, this asymptotic flow depth h_o appears only for $S_o>0$. A particularly simple analysis allows the case $S_o>S_c$ in which S_c is the critical bottom slope for which $h_o=h_c$, thus

$$S_c = \frac{g(1+2h_o/b)^{2/3}}{K^2 h_o^{1/3}} \quad . \tag{88}$$

It is then convenient to consider a rotated coordinate system having a longitudinal coordinate along the (straight) channel bottom and measure flow depths vertically from it. The **pseudo-uniform flow condition** prevails when the energy head H, measured from the channel bottom, remains constant. Far upstream the streamlines are parallel to the channel bottom; consequently, the distribution of pressure is hydrostatic and the velocity distribution is uniform. At the brink zone, however, streamlines are considerably sloped and curved, thereby altering the two respective transverse distributions. As is shown in figure 33, the velocity at the brink section decreases with increasing height, while pressure is atmospheric at the free surface **and** at the channel bottom. Consequently, Eq. (6) must be replaced by the generalized Bernoulli relation (58) accounting for flows with sloped and curved streamlines. For pseudo-uniform flow conditions one may set $z'=z''\equiv 0$ for $x<0$ as outlined above. The resulting solutions for both, the up- and downstream zones of a free overfall are investigated in detail by Hager [19]. In context with discharge measurement, only relations between the far upstream zone and the brink section are sought. The two corresponding flow depths are denoted as h_o and h_e (end depth). It may then be shown that [19]

$$h_e/h_o = \frac{F_o^2}{F_o^2+\frac{2}{5}} \quad , \tag{89}$$

in which $F_o^2=q^2/(gh_o^3)$ is the upstream Froude number. This relation is plotted in figure 34, and it is observed that h_e/h_o ($F_o=1$)$=0.714$ (critical flow conditions at upstream zone), while h_e/h_o($F_o\to\infty$)$\to 1$.

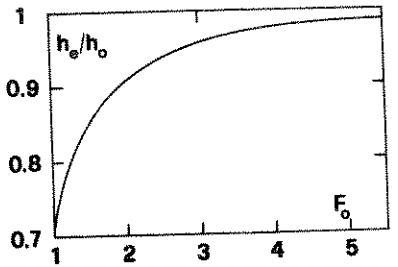

Figure 34 : Ratio between end depth and asymptotic upstream flow depth h_e/h_o as a function of upstream Froude number $F_o=q/\sqrt{gh_o^3}$ in rectangular prismatic channel [19].

Combining Eqs. (85) and (87) yields an expression for the upstream flow depth h_o in terms of parameters h_e/b and

$$\phi = \frac{K^2 h_e^{1/3} S_o}{g} \quad . \tag{90}$$

This is evaluated in figure 35; once the bottom slope S_o and the roughness coefficient K known, and the brink flow depth h_e observed, this plot enables the determination of the asymptotic upstream flow depth h_o. The computation of discharge q per unit width then follows from Eq. (87).

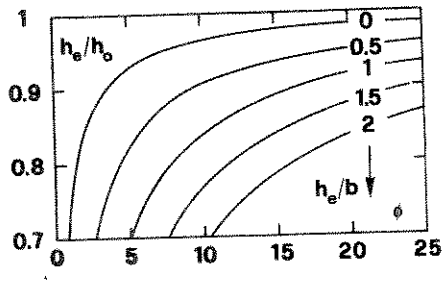

Figure 35 : Relation between non-dimensional brink depth h_e/h_o, ratio h_e/b and $\phi=K^2h_e^{1/3}S_o/g$ for the determination of discharge by using the brink method [19].

Except for the case $F_o=1$, this method of discharge measurement does not account for the critical flow condition. Discharge may only be estimated if the flow depth at a particular location (brink section) **and** the ustream channel characteristics

such as the bottom slope, the roughness coefficient and the width are known.

Example

A rectangular channel having width b=2 m, bottom slope S_o= 0.6 % and roughness coefficient K=1/n=80 $m^{1/3}/s$ according to the Manning-Strickler formula has an end depth h_e=0.73 m (observation). What is the resulting discharge ?

According to Eq. (90) is ϕ=3.52, and h_e/b=0.365, whence from figure 35 h_e/h_o=0.80, thus h_o=0.73/0.8=0.91 m. Inserting this into Eq. (87) yields q=8.16 m^2/s, such that Q=bq=16.3 m^3/s. Critical flow depth is $_oh =(Q^2/(gb^2))^{1/3}$=1.89 m, which is larger than h_o; flow conditions in the approach channel are thus supercritical, as required.

The brink depth method has also been successfully applied on trapezoidal, circular and triangular channels. Particular informations are given by Diskin [11], Smith [54], Rajaratnam and Muralidhar [39] to [41], Neogy [38] and Hager [17].

7.2. Sluice gates

A **sluice gate** is a particular type of an orifice normally situated in a rectangular channel. The gate consists of a thin metal plate and may be placed perpendicularly or oblique to the channel bottom. The top and the bottom edges should be horizontal. The downstream zone of the sluice gate is either of identical geometry as the approach channel (prismatic), or it consists of an enlargement of the cross-sectional area. Also found in hydraulic practice are negative bottom drops at the downstream zone. These latter two are extensively described by Knapp [31]; the following informations refer only to sluice gates in prismatic, horizontal channels.

According to figure 36, distinction must be made between free and submerged flow conditions. For the latter, the downstream flow zone consists of two layers, the upper being a separation zone. Phenomena may be compared with an usual hydraulic jump;

observations indicate no air entrainment. However, to the lowest order of approximation, the free flow condition may be associated with potential flow, while submerged flow conditions reveal considerable local energy dissipation.

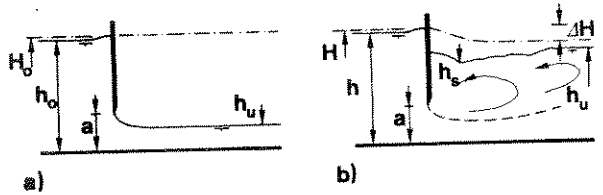

Figure 36 : Plane flow though sluice gate, a) free flow conditions, b) submerged flow conditions. Note the difference in the energy head (-•-)

Let μ be a contraction coefficient, then discharge per unit width for **free sluice gate flow** is [14]

$$q = C_d a\sqrt{2gh_o} \qquad (91)$$

in which

$$C_d = \frac{\mu}{\sqrt{1+\mu a/h_o}} \quad . \qquad (92)$$

The contraction coefficient μ is the ratio between the asymptotic downstream flow depth and the gate opening, $\mu=h_u/a<1$. According to Garbrecht [14], prototype and laboratory measurements indicate

$$C_d = 0.6468(1-\frac{1}{4}\sqrt{a/h_o}) \quad , \qquad (93)$$

while other experimentators, notably Gentilini [16], Rajaratnam et al. [42] provide data for μ. Also, Gentilini investigates the discharge characteristics for inclined and radial sluice gates. The discharge coefficient then augments, the larger the ratio a/h_o and the smaller the angle of the leading edge of the sluice gate with respect to the channel bottom are.

Submerged flow conditions have also been investigated by Garbrecht [14]; the proposed discharge-head relation is

$$q = C_d a\sqrt{2g(h_o - h_s)} \qquad (94)$$

in which h_s is the minimum vertical extension of the downstream height, see figure 36. It has been found that the discharge coefficient C_d is nearly constant and equal to C_d=-0.635. Detailed investigations on the internal flow behaviour are due to Keutner [28], Rajaratnam and Subramanya [43], while Southwell and Vaisey [55], Benjamin [5] and Caulk [9] analyse theoretically the flow structure.

8. CONCLUSIONS

A review of methods for discharge measurement structures indicates that distinction must be made between structures of gradually, moderately and rapidly varied channel geometry. Results for the first class of devices are obtained on a rational basis using the shallow water theory and the critical flow conditions. The latter two types of structures, along which the streamline slope and curvature become significant, behave similarly regarding the qualitative flow process. However, the semi-empirical approach is more useful regarding the quantitative insight into the discharge characteristics. Finally the discharge characteristics of miscellaneous structures such as the free overfall and the sluice gate are given.

9. REFERENCES

[1] Abecassis, F.M., Discussion to "Designing spillway crests for high-head operation", by Cassidy, J.J., Proc. ASCE, **J. Hydraulics Division,** Vol. 96, 1970, 2654-2658.

[2] Abou-Seida, M.M., Quraishi, A.A., "A flow equation for submerged rectangular weirs", **Proc. Inst. Civil Engineers,** Vol. 61, 1976, part. 2, 685-696.

[3] Bazin, H., "Expériences nouvelles sur l'écoulement en déversoir", Dunod, Paris, 1898.

[4] Blau, E., "Die modellmässige Untersuchung von Venturikanaelen verschiedener Groesse und Form", Veroeffentlichungen der Forschungsanstalt fuer Schiffahrt, Wasser- und Grundbau, Akademie Verlag, Berlin, 1960.

[5] Benjamin, T.B., "On the flow in channels when rigid obstacles are placed in the stream", **J. Fluid Mechanics,** Vol. 1, 1956, 227-248.

[6] Bos, M.G., "Discharge measurement structures", Laboratorium voor Hydraulica en Afvoerhydrologie, Landbouwhogeschool, Wageningen, The Netherlands, Rapport 4, May 1976.

[7] Boussinesq, J.M., "Théorie des eaux courantes", Mémoires présentés par divers savants, Académie des Sciences de France, Vol. 23, 1877.

[8] Brestschneider, H., "Abflussvorgaenge bei Wehren mit breiter Krone", Mittl.. Inst. Wasserbau und Wasserwirtschaft, TU Berlin, 53, 1961.

[9] Caulk, D.A., "On the problem of fluid flow under a sluice gate", **Int. J. Engng. Sci.,** Vol. 14, 1976, 1115-1125.

[10] De Coursey, D.E., Blanchard, B.J., "Flow analysis over large triangular weir", Proc. ASCE, **J. Hydraulics Division,** Vol. 96, 1970, HY7, 1435-1454.

[11] Diskin, M.H., "End depth at a drop in trapezoidal channels", Proc. ASCE, **J. Hydraulics Division,** Vol. 87, 1961, HY4, 11-32.

[12] Doeringsfeld, H.A., Barker, C.L., "Pressure-Momentum theory applied to the broad-crested weir", **Trans. ASCE,** Vol. 106, 1941, 934-969.

[13] Forchheimer, P., "Hydraulik", Springer, Heidelberg, Berlin, 1914.

[14] Garbrecht, G., Discussion to "Discharge computations at river control structures", by Collins, D.L., Proc. ASCE, **J. Hydraulics Division,** Vol. 102, 1976, HY12, 1481-1484.

[15] Gentilini, B., "Stramazzi in parete sottile liberi e rigurgitati", **L'Energia Elettrica,** Vol. 13, 1936, 110-132; 245-249; 585-615.

[16] Gentilini, B., "Efflusso dalle luci soggiacenti alle paratoie piane inclinata e a settore", **L'Energia Elettrica,** Vol. 19, 1941; 361-380.

[17] Hager, W.H., "Die Hydraulik von Verteilkanaelen", Thesis presented at the Federal Institute of Technology, ETH, Zurich, Switzerland, Vol 6948, Parts I & II, 1981.

[18] Hager, W.H., Hutter, K., "Approximate treatment of the plane hydraulic jump with separation zone above the flow zone", **J. Hydraulic Research,** Vol. 21, 1983, 195-204.

[19] Hager, W.H., "Hydraulics of plane free overfall", Proc. ASCE, **J. Hydraulic Engineering,** Vol. 109, 1983, HY12, 1683-1697.

[20] Hager, W.H., Hutter, K., "Approximate treatment of plane channel flow", **Acta Mechanica,** Vol. 51, 1984, 31-48.

[21] Hager, W.H., "Abflusserscheinungen in offenen Kanaelen", **Schweizer Ingenieur und Architekt,** Vol. 103, 1985; 252-264.

[22] Hager, W.H., "Critical flow condition in open channel hydraulics", **Acta Mechanica** , Vol. 54, 1985, 157-179.

[23] Hager, W.H., Dupraz, P.-A., "Discharge characteristics of local, discontinuous contractions, I", **J. Hydraulic Research,** Vol. 23, 1985;

[24] Hager, W.H., "Modified Venturi channel", Proc. ASCE, **J. Irrigation and Drainage Engineering,** Vol. 111, 1985, IR1; 19-35.

[25] Hall, G.W., "Analytical determination of the discharge characteristics of broad-crested weirs using boundary layer theory", **Proc. Inst. Civ. Engrs.,** Vol. 22, 1962, 177-190; Vol. 28, 514-548.

[26] Harrison, A.J.M., "The streamlined broad-crested weir", **Proc. Inst. Civ. Engrs.,** Vol. 38, 1967, 657-678; Vol. 41, 1968, 575-599.

[27] Keutner, C., "Stroemungsvorgaenge an breitkronigen Wehrkoerpern und an Einlaufbauwerken", **Bauingenieur,** 1934, Heft 37/38, 366-371; Heft 39/40, 389-392.

[28] Keutner, C., "Wasserabfuehrungsvermoegen von scharfkantigen und abgerundeten Planschuetzen", **Die Bautechnik** ,Vol. 10, 1932, 266-270, 303-305.

[29] Kindsvater, C.E., Carter, R.W., "Discharge characteristics of rectangular thin-plate weirs", Proc. ASCE, **J. Hydraulics Division,** Vol. 83, 1957, HY6, 1453/1-6.

[30] Knapp, R.T., Daily, J.W., Hammitt, F.G., "Cavitation", McGraw-Hill, New York, 1970.

[31] Knapp, F.H., "Ausfluss, Ueberfall und Durchfluss", Verlag G. Braun, Karlsruhe, 1960.

[32] Lemos, F. de Oliveira, "Critérios para o dimensionamento hidraulico de barragens descarregadoras", Lab. Nac. Eng. Civ., Lisboa, 1981.

[33] Lenz, A.T., "Viscosity and surface tension effects on V-notch coefficients", **Trans. ASCE,** Vol. 108, 1943, 759-781.

[34] Mahmood, K., Yevjevich, V., "Unsteady flow in open channels", Vol. 1, Water Resources Publications, Fort Collins, Col. , 1975.

[35] Matthew, G.D., "On the influence of curvature, surface tension and viscosity on flow over round-crested weirs", **Proc. Inst. Civ. Eng.,** Vol. 25, 1963, 511-524.

[36] Misiti, A., "Sullo stramazzo Cipoletti", **L'Acqua,** 1964, Fasc. 1, 1-11.

[37] Moss, W.D., "Flow separation at the upstream edge of a square-edged broad-crested weir", **J. Fluid Mechanics,** Vol. 52, 1972, 307-320.

[38] Neogy, B.N., "Brink depth for trapezoidal broad-crested weir", Proc. ASCE, **J. Hydraulics Division,** Vol. 98, 1972, HY12, 2171-2189.

[39] Rajaratnam, N., Muralidhar, D., "End depth for circular channels", Proc. ASCE, **J. Hydraulics Division,** Vol. 90, 1964, HY2, 99-119.

[40] Rajaratnam, N., Muralidhar, D., "Characteristics of the rectangular free overfall", **J. Hydraulic Research,** Vol. 6, 1968, 233-258.

[41] Rajaratnam, N., Muralidhar, D., "The trapezoidal free overfall", **J. Hydraulic Research,** Vol 10, 1970, 419-447.

[42] Rajaratnam, N., Subramanya, K., "Flow immediately below submerged sluice gate", Proc. ASCE, **J. Hydraulic Division,** Vol. 93, 1967, HY4, 57-77.

[43] Rajaratnam, N., Subramanya, K., "Flow equation for the sluice gate", Proc. ASCE, **J. Irrigation and Drainage Division,** Vol. 93, 1967, IR3, 167-186.

[44] Ramamurthy, A.S., Rao, M.V.J., Auckle, D., "Free flow discharge characteristics of throatless flumes", Proc. ASCE, **J. Irrigation and Drainage Engineering,** Vol. 111, 1985, IR1, 65-75.

[45] Ramponi, F., "Sulle forme di imbocco dei canali e delle opere di scarico superficiali", **L'Energia Elettrica,** Vol. 26, 1949, 453-460.

[46] Rao, N.S.L., "Theory of weirs", Advances in Hydrodynamics, ed. by Ven te Chow, Vol. , 1975.

[47] Rao, N.S.G., Muralidhar, D., "Discharge characteristics of weirs of finite-crest width", **La Houille Blanche,** Vol. 18, 1963, 537-545.

[48] Rao, S.S., Shukla, M.K., "Characteristics of flow over weirs of finite crest width", Proc. ASCE, **J. Hydraulics Division,** Vol. 97, 1971, HY11, 1807-1816; Vol. 98, 1972, HY12, 2224-2231; Vol. 99, 1973, HY7, 1149-1150.

[49] Rehbock, T., "Wassermessung mit scharfkantigen Ueberfaellen", **Zeitschrift VdI,** Vol. 73, 1929, 817-823.

[50] Sarginson, E.J., "The influence of surface tension on weir flow", **J. Hydraulic Research,** Vol. 10, 1972, 431-446; Vol. 11, 1973, 299-306.

[51] Schirmer, A., Diersch, H.-J., "Untersuchungen zum hydraulischen Verhalten von festen, rundkronigen Ueberfaellen bei Ueberbelastung", **Wasserwirtschaft-Wassertechnik,** 1976, 12, 405-412.

[52] Scimeni, E., "Sulla forma delle tracimanti", **L'Energia Elettrica,** Vol. 7, 1930, 293-305.

[53] SIA, "Contribution à l'étude des méthodes de jaugeages", Bull. 18, Schw. Bureau Wasserforschung, Bern, 1926.

[54] Smith, C.D:, "Brink depth for a circular channel", Proc. ASCE, **J. Hydraulics Division,** Vol. 88, 1962, HY6, 125-134; Vol. 89, 1963, HY2, 203-210; HY3, 389-405; HY4, 249-258; HY6, 253-256; Vol. 90, 1964, HY1, 259.

[55] Southwell, R.V., Vaisey, G., "Relaxation methods applied to Engineering problems", **Phil. Trans. A,** Vol. 240, 1946, 117-161.

[56] US Army Engineers, "Hydraulic design of spillways", Engineer Manual, EM 1110-2-1603, Headquarters, Dept. Army, Office of the Chief of Engineers, March, 1965.

[57] Vallentine, H.-R., "Flow in rectangular channels with lateral constriction", **La Houille Blanche,** Vol. 13, 1958, 75-84.

[58] Woodburn, J.G., "Tests of broad-crested weirs", **Trans. ASCE,** Vol. 96, 1932, 387-453.

INDEX